iScience

CellPress
OPEN ACCESS

Article

A LTB_4/CD11b self-amplifying loop drives pyogranuloma formation in chronic granulomatous disease

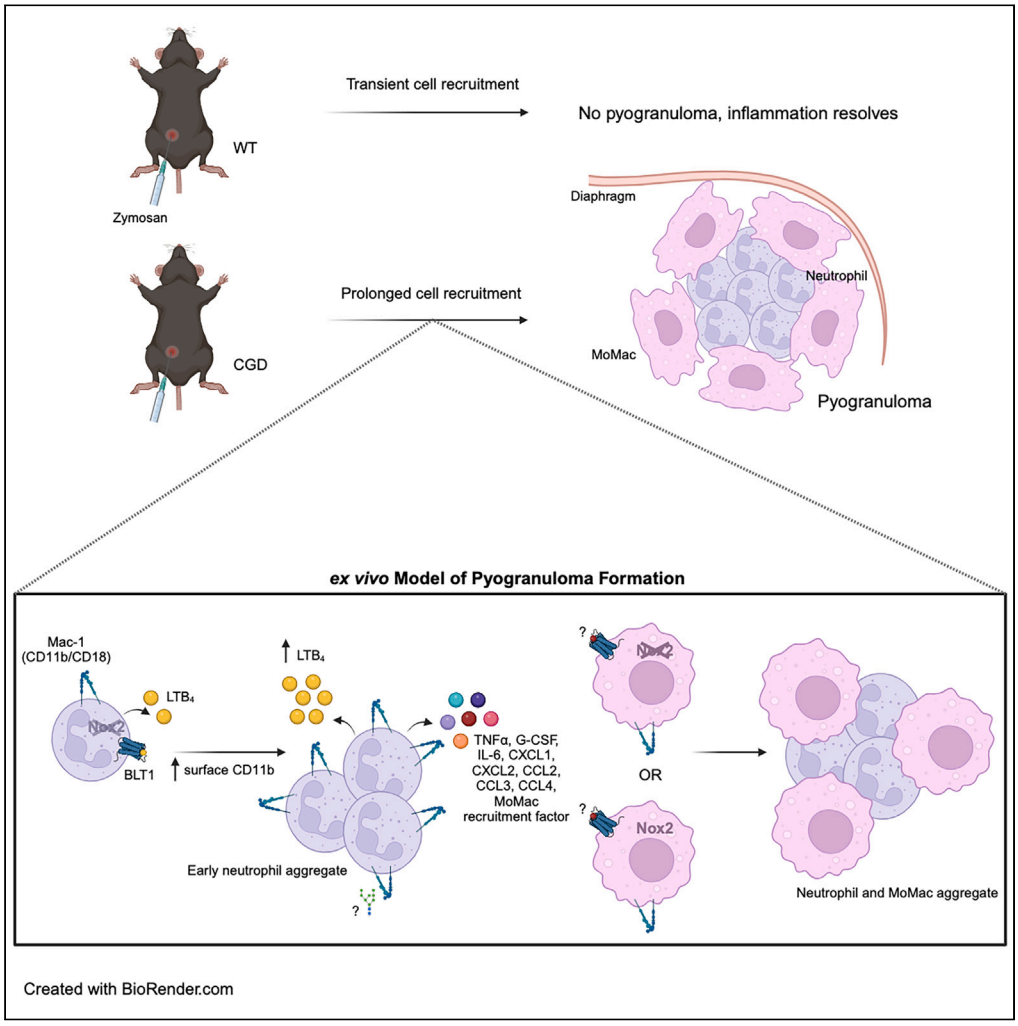

Kelsey C. Haist, Sophie L. Gibbings, Jordan Jacobelli, Kara J. Mould, Peter M. Henson, Donna L. Bratton

haistk@njhealth.org

Highlights

Elevated LTB_4-BLT1 signaling and surface CD11b underlie CGD neutrophil aggregation

Secondary recruitment of MoMacs to CGD neutrophil aggregates is Nox2 independent

MoMac recruitment to CGD neutrophils is not dependent on usual monocyte chemokines

Deficient CD11b leads to disordered neutrophils and few MoMacs in CGD pyogranuloma

Haist et al., iScience 27, 109589
April 19, 2024
https://doi.org/10.1016/j.isci.2024.109589

iScience

CellPress
OPEN ACCESS

Article

A LTB_4/CD11b self-amplifying loop drives pyogranuloma formation in chronic granulomatous disease

Kelsey C. Haist,[1,6,*] Sophie L. Gibbings,[1] Jordan Jacobelli,[2] Kara J. Mould,[3,4] Peter M. Henson,[1,2,3,4] and Donna L. Bratton[1,5]

SUMMARY

Sterile pyogranulomas and heightened cytokine production are hyperinflammatory hallmarks of Chronic Granulomatous Disease (CGD). Using peritoneal cells of zymosan-treated CGD ($gp91^{phox-/-}$) versus wild-type (WT) mice, an *ex vivo* system of pyogranuloma formation was developed to determine factors involved in and consequences of recruitment of neutrophils and monocyte-derived macrophages (MoMacs). Whereas WT cells failed to aggregate, CGD cells formed aggregates containing neutrophils initially, and MoMacs recruited secondarily. LTB_4 was key, as antagonizing BLT1 blocked neutrophil aggregation, but acted only indirectly on MoMac recruitment. LTB_4 upregulated CD11b expression on CGD neutrophils, and the absence/blockade of CD11b inhibited LTB_4 production and cell aggregation. Neutrophil-dependent MoMac recruitment was independent of MoMac Nox2 status, BLT1, CCR1, CCR2, CCR5, CXCR2, and CXCR6. As proof of concept, CD11b-deficient CGD mice developed disrupted pyogranulomas with poorly organized neutrophils and diminished recruitment of MoMacs. Importantly, the disruption of cell aggregation and pyogranuloma formation markedly reduced proinflammatory cytokine production.

INTRODUCTION

Granulomas, often found in the gastrointestinal tract, bladder, and skin, are a hallmark of Chronic Granulomatous Disease (CGD), a primary immunodeficiency resulting from mutations in the NADPH oxidase complex and deficient production of reactive oxygen species. By histopathology, CGD granulomas are categorized as pyogranulomas composed largely of organized collections of neutrophils and macrophages.[1,2] Though patients with CGD suffer from various bacterial and fungal infections,[3] pyogranulomas are often sterile[2,4] and can be induced in murine models of this disease following the instillation of killed aspergillus or zymosan particles made from yeast cell walls into the peritoneum, skin, or lungs.[5–7] As such, CGD pyogranulomas are characteristic of the hyperinflammatory state in this disorder that also frequently results in autoimmunity, inflammatory bowel disease, and poor wound healing.[8–10]

In vitro modeling of granuloma formation has been employed in granulomatous diseases, including tuberculosis and sarcoidosis, and in developing implants and biomaterials, to identify pathogenic mechanisms driving granulomatous reactions and direct potential therapeutic interventions.[11–15] To date, the mechanisms driving pyogranuloma formation in CGD have not been fully investigated.

Here, using $gp91^{phox-/-}$ mice (hereafter, CGD mice), we investigated both *in vivo* pyogranuloma formation during zymosan-induced peritonitis and *ex vivo* modeling using peritoneal inflammatory exudate cells. Time course investigation showed that CGD neutrophils aggregate first and then recruit MoMacs both *in vivo* and *ex vivo*. These events were not seen *in vivo* in wild-type (WT) mice or using WT neutrophils or exudate *ex vivo*. WT MoMacs, however, were recruited with the same efficiency as CGD MoMacs to CGD neutrophil aggregates *ex vivo*. Mechanistically, *ex vivo* modeling demonstrated a self-amplifying loop of LTB_4 production in aggregating CGD neutrophils, as originally described by Song et al.,[16] that, in our model, lead to the upregulation of CD11b on CGD neutrophils and their subsequent ability to recruit MoMacs. This LTB_4/CD11b signaling is an absolute requirement for this process, as its disruption inhibited pyogranuloma formation both *ex vivo* and *in vivo*. Furthermore, CGD cell aggregation was associated with the overproduction of pro-inflammatory cytokines characteristic of CGD, with diminished levels seen following the inhibition of the LTB_4/CD11b signaling loop.

[1]National Jewish Health, Department of Pediatrics, Denver, CO 80206, USA
[2]University of Colorado, Anschutz Medical Campus, Department of Immunology and Microbiology, Barbara Davis Research Center, Aurora, CO 80045, USA
[3]National Jewish Health, Department of Medicine, Denver, CO 80206, USA
[4]University of Colorado, Anschutz Medical Campus, Department of Pulmonary and Critical Care Medicine, Aurora, CO 80045, USA
[5]University of Colorado, Anschutz Medical Campus, Department of Pediatrics, Aurora, CO 80045, USA
[6]Lead contact
*Correspondence: haistk@njhealth.org
https://doi.org/10.1016/j.isci.2024.109589

RESULTS

Ex vivo modeling of *in vivo* pyogranuloma formation

Injection of zymosan into the peritonea of WT or CGD mice resulted in a robust neutrophilia followed by a more gradual rise in the number of MoMacs entering the peritoneal cavity as previously shown.[7] In WT mice, neutrophil and then MoMac numbers subsided after a peak at approximately 18–20 h, and no pyogranulomas developed. Conversely, in CGD mice, there was prolonged recruitment of both neutrophils and MoMacs for days, and many of these cells ultimately accumulated at the diaphragm, a site of peritoneal fluid clearance.[7] Specifically, and as demonstrated previously,[7] the pyogranuloma were found on the peritoneal surface of the diaphragm rather than within the diaphragm structure itself or within lymphatics (Figure 1). Digests of the diaphragm showed that neutrophils began to arrive 6–12 h after zymosan injection and peaked by 24 h, whereas macrophages began to arrive at about 12 h and continued to accumulate over days (Figure 1A). Neutrophils appeared initially as small aggregates that were joined later by macrophages and ultimately organized into discrete organized pyogranulomas[7] that were well-formed by 72 h after i.p. zymosan (Figure 1B). They typically contained a core of neutrophils infiltrated and surrounded by macrophages. We have previously shown that the macrophages recruited to the pyogranulomas are recruited MoMacs, not resident macrophages.[7]

To better dissect the mechanisms driving pyogranuloma formation and investigate its consequences, we sought to develop an *ex vivo* model using plated peritoneal exudate cells from mice 20 h post-zymosan injection, corresponding to the time of peak MoMac recruitment to the peritoneum and a time point in which there was active pyogranuloma formation at the diaphragm in CGD animals. This is also a time point at which MoMacs from each genotype show few differences by RNAseq.[7] As shown from the peritoneal lavage (PL) cellular composition, most cells present in both WT and CGD mice were neutrophils (60–70%), but there was also a substantial population of MoMacs (approximately 20%) at this time point (Figures 1C, S1A, and S1B). Following plating, the CGD cells began to form obvious aggregates by 3 h *ex vivo* that grew to large aggregates with an average area of 400 μm^2 by 24 h similar in size to *in vivo* pyogranuloma (Figures 1C and 1B). Using cells from a Ly6G reporter mouse (Catchup) crossed with a CGD mouse, early nascent aggregates (3 h post-plating) contained predominantly neutrophils (RFP^+), while later aggregates contained both neutrophils and MoMacs ($F4/80^+$) (Figure 1D). This was consistent with the composition of *in vivo* pyogranuloma (Figure 1B), supporting the use of this system as a model of *ex vivo* pyogranuloma formation. Importantly, when these aggregates were stained for markers expressed on other cells present in the lavage, including B cells, NK cells, and T cells, staining for these cells was not seen within the aggregates (Figure S1C), confirming *in vivo* data that neutrophils and MoMacs are the two cell types found within pyogranuloma.[7] Examination of plated WT cells over time showed that no aggregates formed, few WT neutrophils survived 24-h culture, and WT MoMacs remained dispersed (Figure 1C), highlighting that aggregation is a CGD-specific phenomenon.

Since it appeared from an investigation of 20-h CGD PL cells that nascent aggregates of neutrophils initiated the process, we hypothesized that plated CGD neutrophils devoid of signals from CGD MoMacs would also aggregate. To test this, PL cells were obtained at 6 h following zymosan injection, a time when few MoMacs have entered the peritoneum, and plated to observe aggregation. As shown, small aggregates of predominantly early neutrophils were formed in the CGD cultures over 24 h with an average area of 220 μm^2 (Figures 1E and 1F). No aggregates were seen in early WT cultures. In a second approach, 20-h PL cells were almost entirely depleted of MoMacs (<1%), and the neutrophils were plated. Again, much smaller aggregates formed in the CGD cultures, and none formed in the WT (Figure S2).

We also noted that the *ex vivo* cell aggregates did not have the distinct separation of a core of neutrophils surrounded by macrophages (compare Figures 1D with 1B) as seen in pyogranuloma *in vivo*. This was likely reflective of the fact that these aggregates were not formed on the diaphragm surface, a site of peritoneal fluid drainage *in vivo*. Instead, the cell aggregates were rather dynamic structures on plastic in the *ex vivo* setting (see supplemental videos later in discussion), similar to what has been reported for *ex vivo* neutrophil swarms,[17] and rarely exceeded a thickness of a few cells (data not shown). Nevertheless, together, these data suggested that this *ex vivo* system of aggregating CGD neutrophils and MoMacs largely recapitulated the *in vivo* process allowing us to interrogate potential requirements for pyogranuloma formation in an easily manipulated reductionist system.

Next, we sought to define characteristics of MoMacs contributing to their participation in the formation of *ex vivo* pyogranuloma aggregates. Neutrophil-depleted 20-h PL cells were plated and cultured for 24 h. They remained dispersed across the plate or formed rare, loose aggregates (data not shown), demonstrating that CGD neutrophils are required for significant aggregates to form and consistent with prior reports that neutrophils are critical to monocyte activation and participation in swarming events.[18] To formally test whether the presence or absence of $gp91^{phox}$ in MoMacs themselves was required for their recruitment, an assay was devised to enumerate MoMacs recruited to early CGD neutrophil aggregates (Figure 2). Early CGD neutrophils from 6 h PL were plated and allowed to aggregate for an additional 6 h prior to the addition of MoMacs enriched from both WT and CGD 20-h PL cells. As shown in Figure 2, the presence or absence of a functional $gp91^{phox}$ in the MoMacs made no difference in their recruitment to CGD neutrophils (see discussion).

Determining signals for and consequences of CGD cell aggregation in the *ex vivo* model of pyogranuloma formation

Granulomas often occur in response to difficult to digest/indigestible foreign material.[19,20] To this end, we sought to determine whether zymosan particles were driving cell aggregation. Using fluorescent zymosan, 20-h CGD PL cells were imaged over the course of 12 h (Video S1). While zymosan particles were occasionally seen associated with aggregating cells, most aggregates visualized as they formed were not associated with zymosan, although it is possible that this interaction was transient and not captured by imaging every 5 min within a 12-h time-lapse window. Similarly, we hypothesized that dying cells might provide the nidus for cell aggregation as seen in neutrophil swarming.[21] While dying cells stained with SYTOX were sometimes associated with forming aggregates, most aggregates formed without the obvious presence

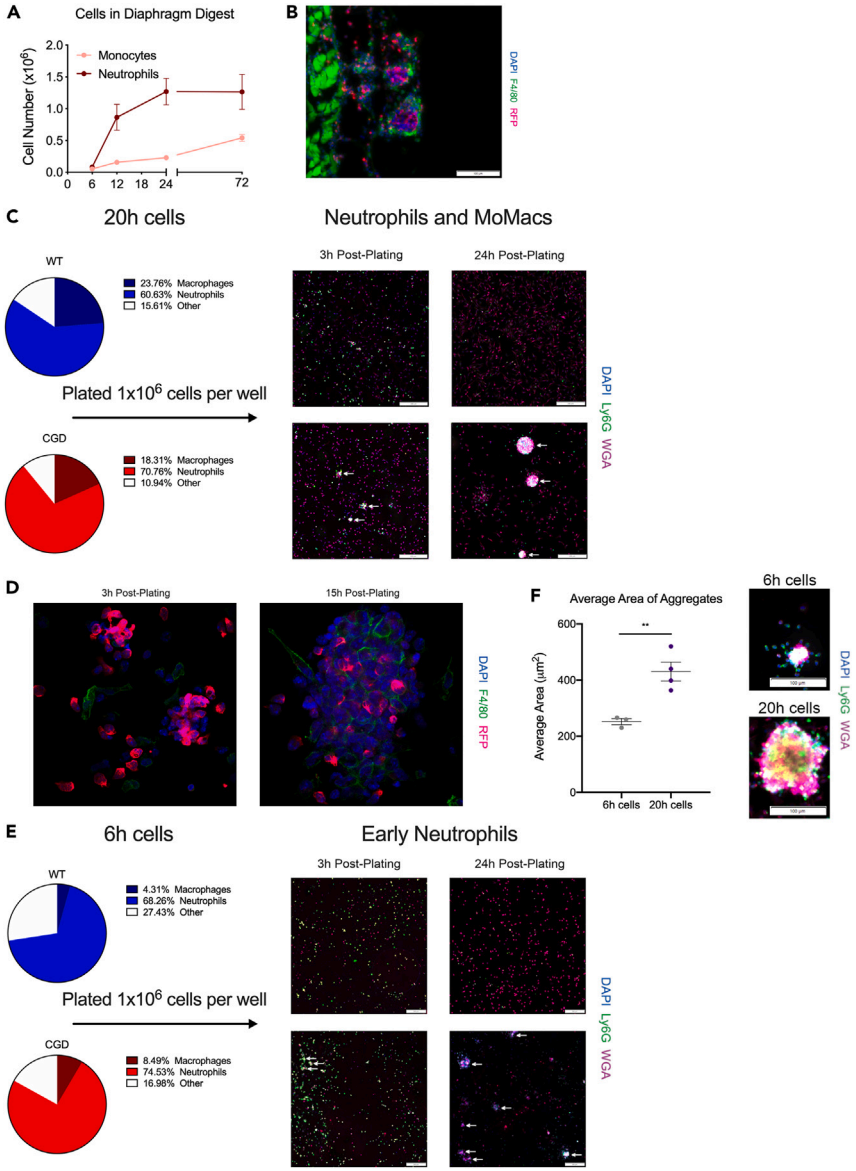

Figure 1. Pyogranuloma formation during zymosan-induced peritonitis is modeled by CGD PL cells *ex vivo*: neutrophil aggregation is followed by MoMac recruitment

(A) Neutrophils and then MoMacs accumulate at the diaphragm after i.p. zymosan. CGD diaphragms were digested at the indicated times and cells analyzed by flow cytometry.

(B) Pyogranuloma at the diaphragm 72 h after i.p. zymosan in Catchup x CGD mice. Neutrophils are RFP^+ and MoMacs $F4/80^+$. Sections were imaged at 40× magnification using an Olympus VS200 microscope. Green at left is autofluorescence of smooth muscle.

(C) 20-h PL cells from WT and CGD mice were typed by flow cytometry (pie chart) and 10^6 cells plated on cover slips. N = 4 mice, 4 experiments. Coverslips were fixed at the times indicated, stained with WGA, anti-Ly6G, and DAPI, and imaged at 10× magnification using an Olympus VS200 microscope. Arrows indicate representative aggregates. Scale bar is 200 μm.

(D) 20-h PL cells from Catchup × CGD mice were plated, processed, and stained as above, and aggregates were imaged at 40× magnification using a Zeiss LSM confocal microscope.

(E) 6-h PL cells were plated and analyzed as in (C). N = 3 mice, 3 experiments.

(F) 6-h and 20-h PL cells were processed as in (C) and (E) and aggregate size quantified after 24 h in culture. Four images were analyzed per coverslip using Imaris software to define the average size of the aggregates detected. N = 3–4 mice, from 3 to 4 experiments. *p* values were determined by t-test. $^{**}p < 0.01$. Microscopy images show a representative 6-h (top) and 20-h (bottom) aggregate. Scale bar is 100 μm.

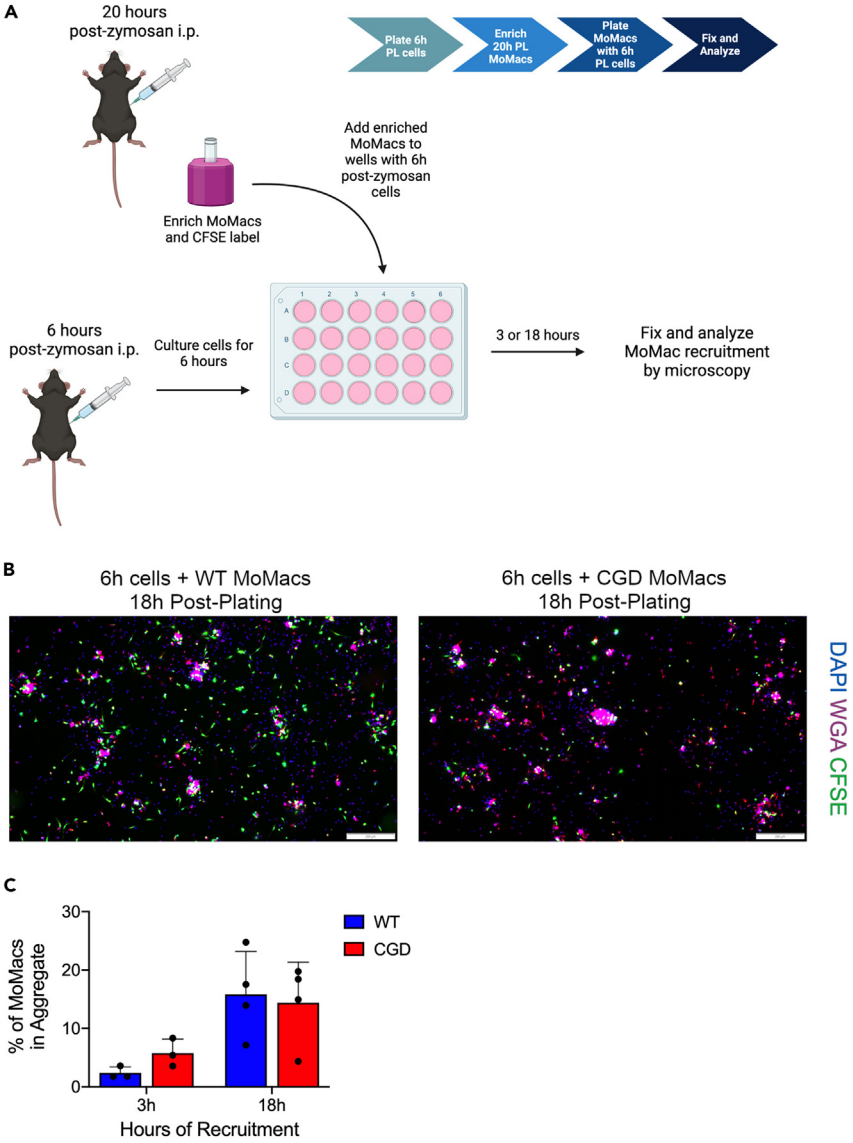

Figure 2. WT and CGD MoMacs are both recruited to CGD early neutrophil aggregates

(A) Experimental setup to show MoMac recruitment to CGD neutrophil aggregates. 6-h PL cells from CGD mice were plated for 6 h prior to the addition of CFSE-labeled enriched 20-h WT or CGD PL MoMacs. Resulting aggregates were analyzed after 3 or 18 h of culture. Coverslips were fixed, stained with anti-Ly6G and DAPI, and imaged at 10× using an Olympus VS200 microscope.

(B) Representative images of WT and CGD CFSE-labeled MoMacs plated with CGD neutrophil aggregates. Scale bar is 200 μm.

(C) Quantification of microscopy images. Four images were analyzed per coverslip using Imaris software to define aggregates and CFSE-labeled MoMacs. MoMacs were then defined as within or not within an aggregates and percent within an aggregate was calculated. N = 3–4 mice, from 3 to 4 experiments. *p* values were determined by multiple t-tests.

of a dying cell (Video S2). These data suggest that neither zymosan particles nor dying cells are explicitly required in the formation of aggregates.

Given the importance of neutrophils to the aggregation process, we next sought to assess the role of various neutrophil chemoattractants in the aggregation process. Aggregation of PL cells was performed in the presence of an antagonist cocktail targeting important neutrophil chemoattractant receptors including CXCR1, CXCR2, FPR1, FPR2, and BLT1, which robustly inhibited aggregation (Figures S3A and S3C). Breaking down the individual components of the cocktail was illustrative: treatment of PL cells with the individual components directed at CXCR1, CXCR2, and FPR2 showed no inhibition (Figures S3B and S3D). One antagonist to FPR1 (cyclosporin H), showed minimal but significant inhibition only on 6-h PL cells, suggesting that FPR1 may contribute a minor role in neutrophil aggregation. When we focused on LTB_4 signaling, we saw significant inhibition of aggregation by U75302, acting as a competitive antagonist on BLT1, with minimal contribution from

LY255283, a known BLT2 antagonist (Figure 3A). Notably, the BLT2 receptor is not expressed on murine neutrophils and macrophages.[22] It has been reported that, at higher doses above 10 μM, LY255283 acts as a noncompetitive antagonist of BLT1.[23–25] Thus, by using a high dose of LY255283 (83.3 μM) along with the BLT1 competitive inhibitor U75302, we aimed to fully antagonize BLT1. Together, these antagonists almost completely inhibited the aggregation of early neutrophils obtained at 6 h following zymosan administration (Figure 3B). Furthermore, consistent with an important role for LTB_4 in this process, LTB_4 levels were significantly elevated in PL fluid of CGD compared to WT mice following zymosan administration (Figure S3E) and were elevated in supernatants following 24-h culture of CGD PL cells (Figure 3C). In total, these data strongly implicated LTB_4 as a primary driver of cell aggregation in this system and corroborate substantial early data: LTB_4 is known to be critical for neutrophil swarming responses,[21] and Song et al. published that its heightened production drives initial neutrophil migration into CGD murine lungs following zymosan instillation and self-adhesive aggregation of TNFα-primed CGD bone marrow neutrophils.[16] As such, we sought to define the downstream mechanisms by which LTB_4 acts in pyogranuloma formation.

As earlier work had shown the expression of BLT1 (but not BLT2) by MoMacs,[7] we tested whether LTB_4 might also be a significant chemoattractant for MoMacs to the aggregates. Notably, the antagonists U75302 and LY255283 robustly inhibited the aggregation of 20 h PL cells consisting of MoMacs and neutrophils (Figure 3D). Using early CGD neutrophils as the initial aggregating cells as in Figure 2, enriched MoMacs from WT and $BLT1^{-/-}$ mice showed equivalent recruitment to aggregates (Figure 3E). Similarly, both WT and $BLT1^{-/-}$ MoMacs migrated comparably in a transwell system in response to conditioned media generated by 6-h PL cells (Figures S3F and S3G). In summary, LTB_4 appears to be critical in this model of *ex vivo* pyogranuloma formation by functioning at the level of initiating neutrophil aggregation, but not for the recruitment of MoMacs.

It was hypothesized that CGD cell aggregates serve as a driver of proinflammatory mediator production and that the disruption of aggregates by antagonizing LTB_4 signaling would lessen this hyperinflammatory response by CGD cells in *ex vivo* culture. To this end, supernatants were collected from 6-h and 20-h CGD PL cells cultured *ex vivo* for 24 h with or without the BLT1 and BLT2 antagonists and various cytokine levels measured by multiplex and ELISA. Culture of either 6-h or 20-h CGD PL cells with the BLT1 and BLT2 antagonists resulted in significantly lower levels of TNFα, G-CSF, CXCL1, CXCL2, IL-6, CCL2, CCL3, and CCL4 in *ex vivo* culture supernatants (Figure 3E), demonstrating that the disruption of LTB_4 signaling did lessen the hyperinflammatory response of CGD cells, potentially through the inhibition of aggregation.

Given the high levels of potential MoMac chemoattractants made by CGD cells, their role in MoMac recruitment to CGD neutrophil aggregates was next assessed. Conditioned media from 20-h PL CGD cells was generated following overnight culture and again high levels of CCL2, CCL3, and especially CCL4 were detected (Figure 4A). MoMac recruitment to early neutrophil aggregates, as in Figure 2, showed no inhibition for either WT or $BLT1^{-/-}$ MoMacs when treated with antibodies to these chemokines (Figure 4B) in quantities demonstrated to neutralize them effectively (data not shown). Similarly, these neutralizing antibodies had no effect on the migration of the MoMacs in the transwell system (Figures S4A and S4B).

Having shown that these classical MoMac chemoattractants appeared to play no role in their recruitment to CGD cell aggregates, we took a step back to further characterize potential mediators for MoMac attraction. Transwell experiments using either proteinase K-treated or size-fractionated conditioned media demonstrated that a protein factor(s) greater than 5 kDa in size was key (Figure S4C). Given that typical CC and CXC chemokines are around 8–12 kDa in size, we used our RNAseq data[7] to determine the canonical chemokine receptors most robustly expressed on MoMacs, both WT and CGD, that could potentially mediate their recruitment to aggregates. Based on the expression of CCR1, CCR2, CCR5, CXCR2, and CXCR6, transwell experiments using blockade of each of these via either antagonists or blocking antibodies were performed and again, no impact on MoMac migration to conditioned media was seen (Figure S4D). As of yet, the protein factor(s) responsible for attracting MoMacs into the aggregates have not been elucidated (see discussion).

CD11b signals downstream of LTB_4 to enhance cell aggregation *ex vivo* and *in vivo* pyogranuloma formation and is key to CGD pro-inflammatory cytokine production

Next, signals downstream of heightened LTB_4 production important to CGD cell aggregation were investigated. LTB_4 has been shown to upregulate CD11b,[26,27] and as CD11b is an important α-integrin expressed on myeloid cells including neutrophils and MoMacs, CD11b levels on neutrophils and MoMacs from peritoneal lavage in zymosan-treated mice were assessed. CD11b levels were higher on CGD PL neutrophils compared to WT, but no genotype differences were seen for MoMac CD11b levels (Figure 5A). Furthermore, when CGD exudate cells were treated with BLT1 and BLT2 antagonists in culture for 24 h, there was decreased CD11b expression on the neutrophils (Figure 5B), supporting that LTB_4 contributes to increased CD11b expression on CGD neutrophils. There was no impact on MoMac CD11b levels (data not shown). To determine the role of CD11b in aggregation in the *ex vivo* pyogranuloma model, a blocking anti-CD11b antibody was added to 20-h aggregating CGD neutrophils and MoMacs (Figure 5C). The blockade of CD11b led to a significant reduction in the number of aggregates and reduction in their size. Given that MoMac recruitment is dependent on neutrophil aggregation, the antibody was also assessed for the disruption of the aggregation of early neutrophils obtained 6 h after zymosan. Blockade here resulted in almost complete abrogation of early neutrophil aggregates. To assess effects specifically on MoMacs recruited to the aggregates, 20-h MoMacs from WT, $CD11b^{-/-}$, CGD, and $CD11b^{-/-}$ CGD mice were enriched and added to aggregating 6-h early neutrophils from CGD mice treated with zymosan as in Figure 2. As shown in Figure 5D, minimal inhibition of MoMac recruitment was seen in the absence of CD11b. Additionally, cells plated from CGD mice that lacked CD11b expression produce less LTB_4 after 24 h in culture (Figure 5E), demonstrating the requirement for CD11b in the feedforward mechanism that drives LTB_4 production. Together, these data suggest that CD11b is upregulated downstream of LTB_4 on CGD neutrophils, is critical to their aggregation, and results in the production of more LTB_4.

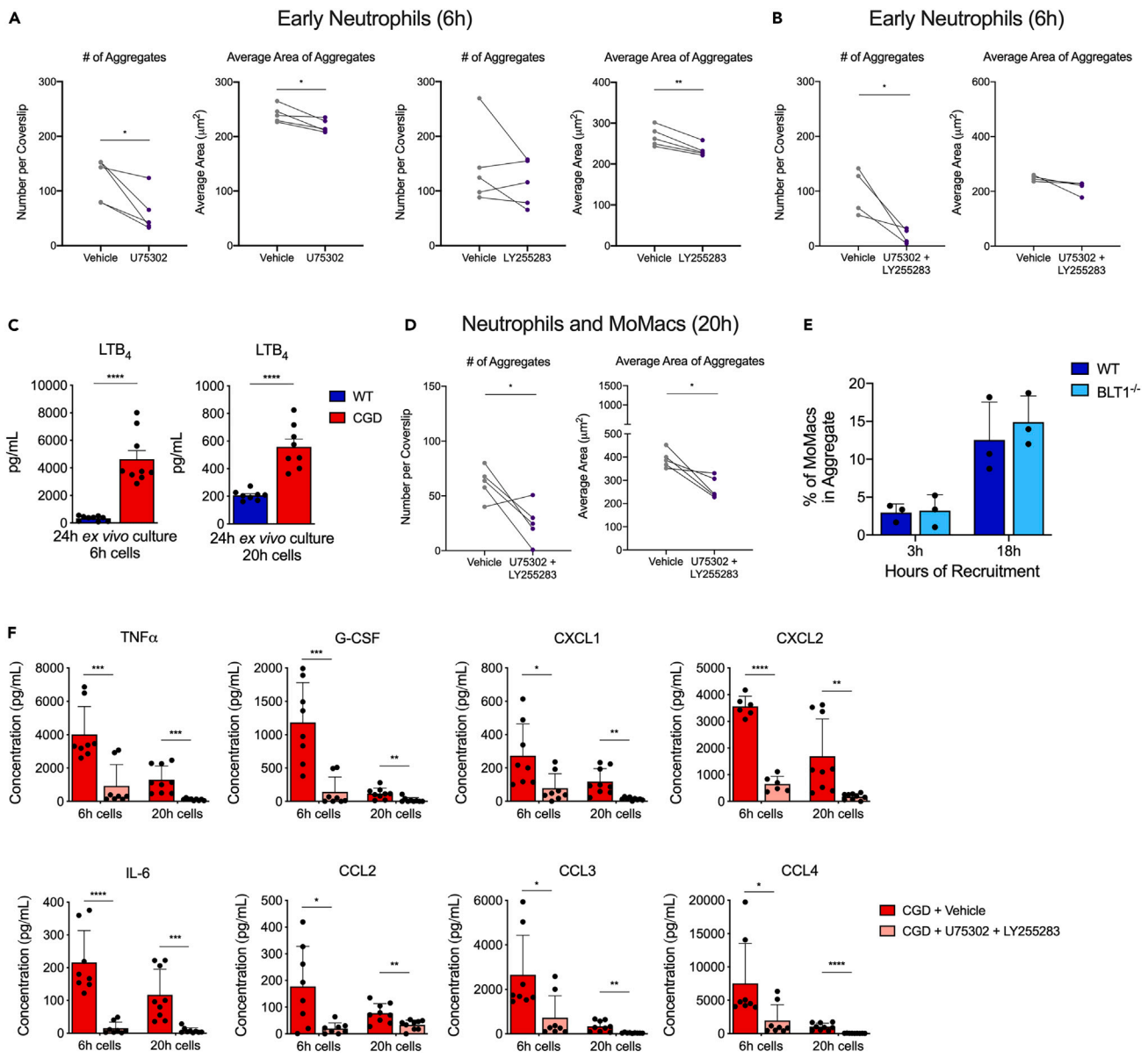

Figure 3. LTB_4 mediates the *ex vivo* aggregation of peritoneal lavage cells from zymosan-treated CGD mice via the aggregation of neutrophils

(A and B) PL cells were harvested at 6 h post-zymosan, plated, cultured for 24 h with either vehicle or LTB_4 receptor antagonists together (A) or individually (B), fixed, stained and imaged as in Figure 1C. Four images were analyzed per coverslip using Imaris software to define the number of aggregates within the image and the average size of the aggregates detected. N = 4–5 mice, from 2 to 5 experiments. *p* values were determined by paired t-test. *p < 0.05, **p < 0.01.

(C) LTB_4 in conditioned media was measured by ELISA following 24-h culture of 6-h (left) and 20-h (right) PL cells. N = 8–9 samples, from 3 experiments. *p* values were determined by multiple t-tests. ****p < 0.0001.

(D) PL cells were harvested at 20 h post-zymosan, plated, cultured for 24 h with either vehicle or both LTB_4 receptor antagonists, fixed, stained and imaged as in Figure 1C. Four images were analyzed per coverslip using Imaris software to define the number of aggregates within the image and the average size of the aggregates detected. N = 5 mice, from 5 experiments. *p* values were determined by paired t-test. *p < 0.05.

(E) Labeled MoMacs from WT and $BLT1^{-/-}$ mice were recruited to aggregates initiated by 6-h CGD PL cells and were quantified as in Figure 2. N = 3 mice, from 3 experiments. *p* values were determined by multiple t-tests.

(F) TNFα, G-CSF, CXCL1, CXCL2, IL-6, CCL2, CCL3, and CCL4 were measured by multiplex or by ELISA following 24-h culture of 6-h or 20-h CGD PL cells cultured in the presence of vehicle or BLT1 and BLT2 antagonists. N = 6–9 samples, from 3 experiments. *p* values were determined by multiple t-tests. *p < 0.05, **p < 0.01, ***p < 0.001, ****p < 0.0001.

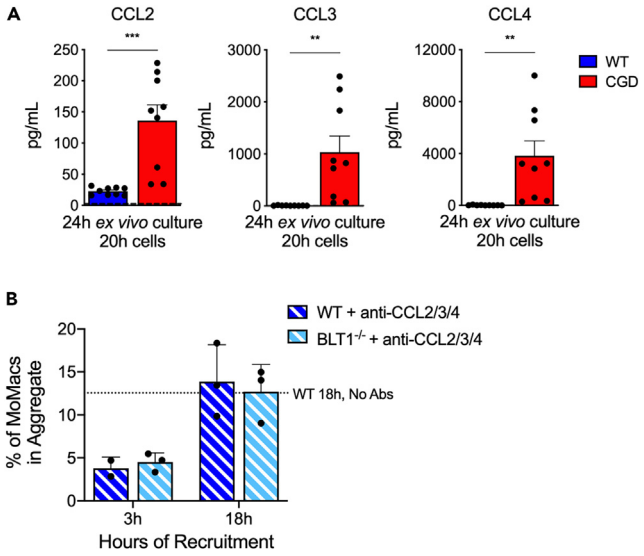

Figure 4. Neither CCL2, CCL3, CCL4 nor LTB_4 mediate the recruitment of MoMacs to CGD aggregates

(A) Levels of CCL2, CCL3, and CCL4 in conditioned media after 24-h culture of 20-h peritoneal lavage cells were measured by multiplex assay. N = 9 samples, from 3 experiments. *p* values were determined by t-test. **p < 0.01, ***p < 0.001.

(B) Recruitment of labeled WT and $BLT1^{-/-}$ enriched MoMacs into CGD 6-h PL neutrophil aggregates in the presence of anti-CCL2/3/4 antibodies was assessed and analyzed as in Figure 2. Dotted line represents WT MoMacs found in the aggregates after 18 h in culture in the absence of the antibodies. N = 3 mice, from 3 experiments. *p* values were determined by multiple t-tests.

It was also hypothesized that preventing aggregation at the level of CD11b would diminish the production of proinflammatory cytokines similar to that seen in CGD cells cultured in the presence of BLT1 and BLT2 antagonists (above). To address this, supernatants were collected from 6-h and 20-h CGD and $CD11b^{-/-}$ CGD PL cells cultured *ex vivo* for 24 h and levels of the various cytokines and chemokines measured by multiplex and ELISA. We saw significantly lower levels of TNFα, G-CSF, CXCL1, CXCL2, IL-6, CCL2, CCL3, and CCL4 in 20-h $CD11b^{-/-}$ CGD *ex vivo* supernatants and significantly lower levels of all but CCL2 and IL-6 in 6-h supernatants (Figure 5F). These data suggest that the disruption of aggregation via the absence of CD11b on CGD cells, as with antagonism of LTB_4 signaling, lessens the hyperinflammatory response of CGD cells, highlighting the importance of aggregation specifically to this CGD phenomenon.

Next, potential ligand(s) for CD11b contributing to the aggregation of CGD cells in this system were investigated. Ligands of CD11b/CD18, fibrin, C3b, and ICAM-1 or indirect partners (CD61 on platelets binding to fibrin that binds to CD11b) were assessed by flow cytometry.[28,29] CGD neutrophils from 6-h PL showed the expression of all 4 proteins (Figure S5A). Then, the aggregation of PL cells, both early neutrophils and mixed neutrophil/MoMac cultures in the presence of blocking antibodies or peptides to various CD11b ligands including fibrin(ogen), ICAM-1, and C3b was assessed. Blockade of these ligands did not appreciably alter aggregation (Figures S5B and S5C; and see discussion).

Given this evidence of an LTB_4/CD11b self-amplifying loop driving the aggregation of CGD neutrophils, which in turn recruits MoMacs in this *ex vivo* pyogranuloma model, we hypothesized that targeting this amplification loop would disrupt pyogranuloma formation *in vivo*. To this end, $CD11b^{-/-}$ CGD mice were used to disrupt the amplification loop because CD11b is not required for entry into the peritoneum,[30] and it was hypothesized that the complete disruption of the LTB_4 signal would almost certainly prevent early neutrophil recruitment to the peritoneum.[16] First, it was established whether initial cell recruitment was altered, and as demonstrated at 24 h, no differences were seen between the $CD11b^{-/-}$ CGD and CGD mice in the numbers of neutrophils and MoMacs recruited to the peritoneum (Figure 6A). By 72 h, however, neutrophil numbers in PL were decreased in the $CD11b^{-/-}$ CGD mice relative to CGD mice (Figure 6A). While MoMac numbers were decreased in $CD11b^{-/-}$ CGD mice in PL at 72 h, this decrease was not statistically significant. The decreases in neutrophil and MoMac numbers were not due to an increase in cell death, as the percentages of necrotic and apoptotic cells at both 24 and 72 h were quite low in all genotypes (less than 7.5%; data not shown) as previously published.[7] Similar to *ex vivo* cultures, it was hypothesized that $CD11b^{-/-}$ CGD mice would also have lower levels of proinflammatory cytokines and chemokines in PL fluid relative to CGD mice, consistent with a decreased hyperinflammatory response. To test this, the levels of cytokines and chemokines in PL fluid from these mice was measured and significantly lower levels of TNFα, G-CSF, CCL2, and CCL4 were found in the lavage fluid from $CD11b^{-/-}$ CGD mice relative to CGD mice (Figure 6B), suggesting that the hyperinflammatory response was diminished in these mice.

Having demonstrated that these mice exhibited a reduced hyperinflammatory phenotype similar to the *ex vivo* cultures, it was also hypothesized that these mice would have reduced pyogranuloma formation consistent with the reduced aggregation seen *ex vivo*. $CD11b^{-/-}$ CGD mice had fewer neutrophils and MoMacs at the diaphragm compared to CGD mice (Figure 6C). Assessing pyogranuloma formation at the

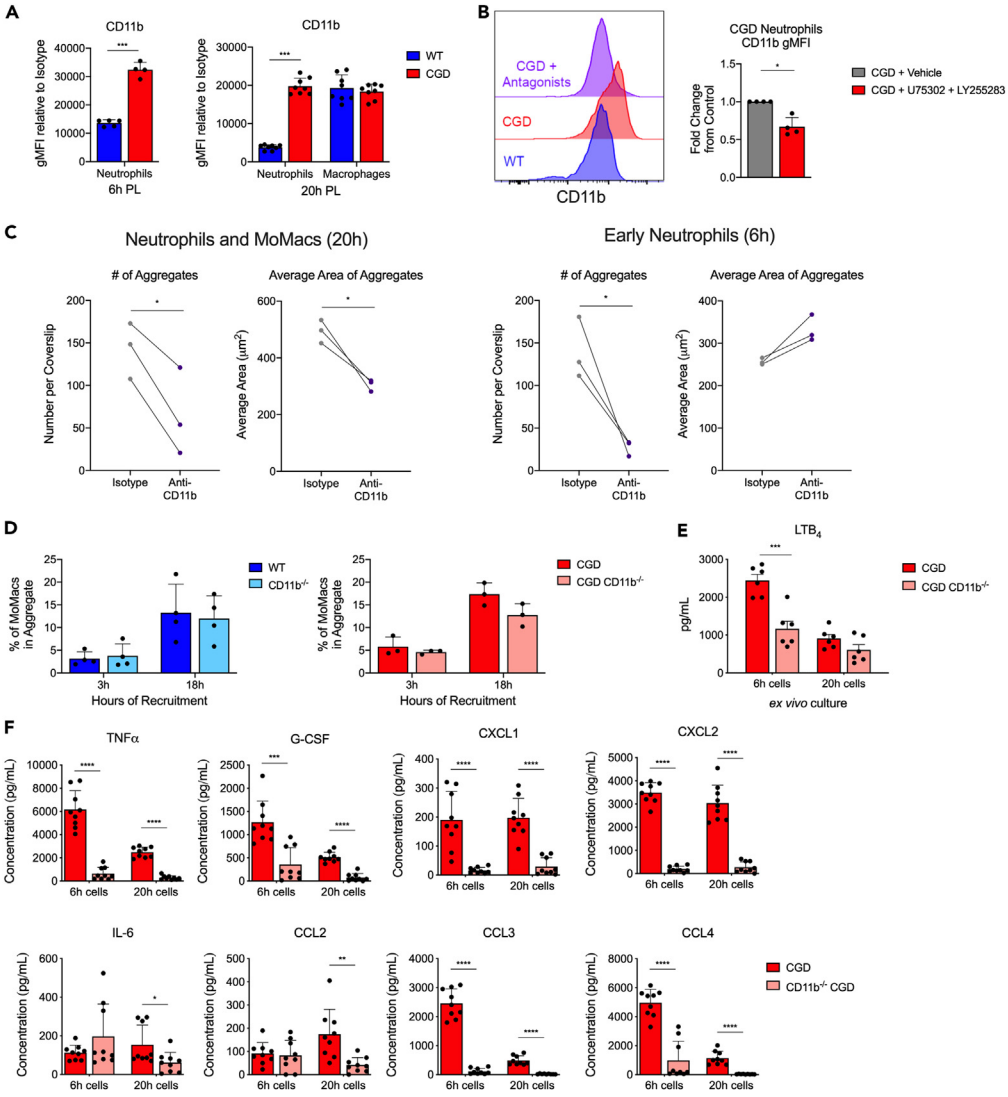

Figure 5. CD11b expression on neutrophils is elevated in CGD, lowered by LTB_4 receptor antagonists, and mediates the aggregation of peritoneal lavage cells *ex vivo*

(A) CD11b surface expression was measured by flow cytometry on 6-h PL neutrophils (left) and 20-h PL neutrophils and MoMacs (right) post-zymosan. N = 4–8 mice, from 2 to 3 experiments. *p* values were determined by multiple t-tests. ***p < 0.001.

(B) CD11b expression was measured on 20-h PL neutrophils after 24 h culture with vehicle or the LTB4 receptor antagonists. N = 4 mice, from 3 experiments. *p* values were determined by paired t-test. *p < 0.05.

(C) CGD PL cells were harvested at 20 h and 6 h post-zymosan and allowed to aggregate with or without blocking anti-CD11b antibody and analyzed as in Figures 3B and 3C. N = 3 mice, from 3 experiments. *p* values were determined by paired t-test. *p < 0.05.

(D) Recruitment of WT and CD11b$^{-/-}$ (left) and CGD and CD11b$^{-/-}$ CGD (right) enriched MoMacs into CGD 6-h PL neutrophil aggregates was performed and analyzed as in Figure 2. N = 3–4 mice, from 3 to 4 experiments. *p* values were determined by multiple t-tests.

(E) Levels of LTB_4 in cell culture supernatants after 24-h culture of 6-h (left) and 20-h (right) PL cells as measured by ELISA. N = 6 samples, from 2 experiments. *p* values were determined by multiple t-tests. ***p < 0.001.

(F) TNFα, G-CSF, CXCL1, CXCL2, IL-6, CCL2, CCL3, and CCL4 were measured by multiplex or by ELISA following 24-h culture of 6-h or 20-h CGD or CD11b$^{-/-}$ CGD cells. N = 9 samples, from 3 experiments. *p* values were determined by multiple t-tests. *p < 0.05, **p < 0.01, ***p < 0.001, ****p < 0.0001.

diaphragm, the CGD mice had well-formed pyogranuloma composed of neutrophils surrounded by MoMacs as expected (Figure 6D). In contrast and as hypothesized, the CD11b$^{-/-}$ CGD mice showed poor pyogranuloma formation. While many neutrophils were localized to the peritoneal side of the diaphragm, they exhibited little organization or at best loose aggregations with a paucity of MoMacs recruited to their vicinity. These data demonstrate that CD11b is key to pyogranuloma formation *in vivo* and the hyperinflammatory response that occurs in CGD mice after an inflammatory stimulus.

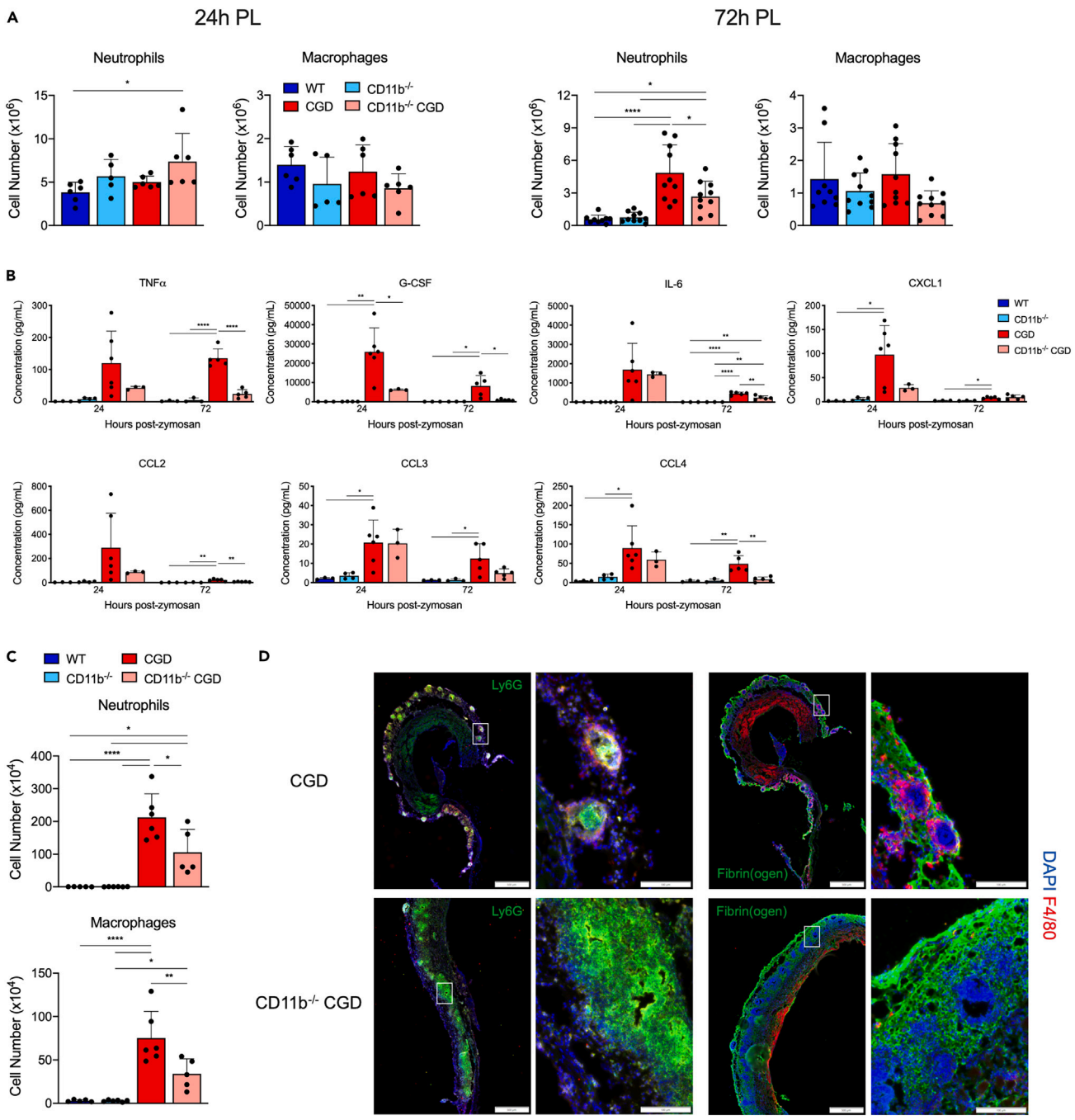

Figure 6. Absence of CD11b in CGD mice disrupts pyogranuloma formation at the diaphragm and is associated with the reduced production of pro-inflammatory cytokines/chemokines following ip zymosan

WT, CGD, CD11b$^{-/-}$, and CD11b$^{-/-}$ CGD mice were treated with i.p. zymosan and harvested at 24 and 72 h post-zymosan.

(A) Numbers of neutrophils and MoMacs post-zymosan were quantified by flow cytometry in PL at 24 and 72 h. N = 5–10 mice, from 2 to 3 experiments. *p* values were determined by one-way ANOVA with a Tukey's multiple comparisons test. *p < 0.05, ****p < 0.0001.

(B) Multiplex analysis of PL fluid at 24 and 72 h. *p* values were determined by one-way ANOVA with a Tukey's multiple comparisons test. *p < 0.05, **p < 0.01, ****p < 0.0001.

(C) Numbers of neutrophils and MoMacs in diaphragm digests were quantified by flow cytometry at 24 and 72 h post-zymosan. *p* values were determined by one-way ANOVA with a Tukey's multiple comparisons test. *p < 0.05, **p < 0.01, ****p < 0.0001.

(D) 72-h diaphragms were harvested, fixed, and frozen prior to sectioning. Sections were stained as shown and imaged at 20× using an Olympus VS200. Peritoneal side of the diaphragm is on the left side in all left-hand images. Areas denoted by a white box in left-hand images are shown enlarged in right-hand images.

DISCUSSION

Even as gene therapy for CGD becomes a reality, many of the hyperinflammatory aspects of the disease may persist until such therapy is optimized.[31] As such, a more thorough understanding of the underlying mechanisms driving hyperinflammation are of clinical value. CGD pyogranulomas obstruct viscera, cause organ dysfunction, and, based on our data, such cell aggregates are likely important in the excessive production of cytokines characteristic of CGD. Current therapy for pyogranulomas is generally untargeted, e.g., corticosteroids and azathioprine.[2,32] We sought to investigate pyogranuloma formation first *in vivo* and then devised an *ex vivo* model to interrogate underlying mechanisms. CGD pyogranulomas likely begin as an innate response to tissue injury or to contain initial invading pathogens. Nevertheless, they are usually sterile when assessed clinically with the persistence of neutrophils and macrophages as organized structures the most salient feature. Several contributing factors are hypothesized: heightened longevity and poor signaling by CGD neutrophils for clearance, and deficient efferocytosis by improperly programmed CGD macrophages.[30,33–36] Slowed digestion of pathogens, tissue debris, and apoptotic cells resulting from improper acidification and activation of proteases in phagolysosomes may also contribute.[33,37,38]

It is hypothesized that CGD pyogranuloma formation results from an aberrant swarming response. In the normal host, pioneer neutrophils migrate toward pathogen-derived stimuli or DAMPs,[39–42] recruiting more neutrophils via key amplifying signals including LTB_4.[21,43,44] The subsequent recruitment of macrophages leads to swarm resolution, making this a transient process[44,45] with the LTB_4 amplification loop ultimately self-limited by NADPH oxidase activity.[46] LTB_4 signaling appears to be heightened in CGD, where loss of NADPH oxidase activity fails to inhibit the production of LTB_4[46] and cell aggregation results in the heightened transcellular production of LTB_4.[47] LTB_4 is of particular importance in innate responses to fungal pathogens generally[47–50] and, in CGD mice, has been shown to be the key chemoattractant for early neutrophil recruitment following zymosan installation and the initiator of bone marrow neutrophil aggregation.[16] As such, antagonizing LTB_4 signaling in this model of pyogranuloma formation was potently inhibitory. Further dissection revealed that LTB_4 was acting solely at the level of neutrophil aggregation and not at the level of MoMac recruitment, despite their expression of BLT1.[7]

MoMac recruitment to aggregates appeared to be secondary, recapitulating the time course of pyogranuloma formation *in vivo*. Intrinsic expression of Nox2, or lack thereof, did not alter MoMac recruitment to the aggregating CGD neutrophils. This observation that MoMacs, either WT or CGD, demonstrated significant plasticity by responding to their milieu is reminiscent of our previous work.[7] A limitation of the current study was our inability to determine the neutrophil-derived protein factor(s) that recruit MoMacs. The monocyte-attracting chemokines CCL2, CCL3, and CCL4 are produced at high levels in the zymosan-inflamed peritoneum and in media conditioned by CGD neutrophils. These chemokines act through CCR2, CCR1, and CCR5, respectively, which are well expressed by WT and CGD 20-h MoMacs by RNAseq.[7] CCR2 is known to play a central role in the recruitment of monocytes from blood into the peritoneum and for the recruitment of MoMacs to neutrophil clusters *in vivo*.[45,51] Nonetheless, targeting these chemokines and receptors in our *ex vivo* model of aggregation and in transwell experiments did not indicate a role for these as signals for MoMac recruitment to the neutrophil aggregates, and as yet, key mediator(s) have not been identified.

Given the persistent nature of the cell aggregates, we hypothesized that adhesive molecules, such as integrins were involved in the stabilization process. The α-integrin CD11b together with the β_2 integrin CD18 forms the CR3/Mac-1 complex that is expressed on both neutrophils and MoMacs. CD11b expression level is known to be increased by LTB_4.[26,27] We thus posited that CD11b was involved in the formation and stabilization of aggregates. Disrupting its signaling was quite effective in inhibiting neutrophil and MoMac aggregation in the *ex vivo* pyogranuloma model. Notably, however, as with the antagonism of LTB_4, CD11b appeared to act at the level of disrupting early neutrophil aggregates, thereby inhibiting MoMac recruitment indirectly. Importantly, blockade of CD11b did reduce the amount of LTB_4 produced by the neutrophil aggregates possibly by disrupting its transcellular production.[47] Thus, a feedforward loop is apparent: LTB_4 upregulates CD11b on CGD neutrophils, which enhances their aggregation and LTB_4 production. This corroborates the findings of Song et al.,[16] where the CGD neutrophil production of LTB_4 was dependent on cell density. While a search for CD11b ligands proved unproductive, β-glucan, a major component of zymosan particles, has also been shown to bind to CD11b[52] and is still a possibility. Although we did not find a requirement for zymosan particles as a nidus for forming aggregates in live cell time-lapse imaging experiments, it is possible that β-glucan freed from zymosan particles is bound by CD11b and propagates inflammatory signaling. Importantly, the disruption of aggregation either by antagonism of LTB_4 or CD11b both *ex vivo* and *in vivo* reduced the output of many proinflammatory cytokines characteristic of CGD.

We hypothesized that the disruption of this feedforward loop in CGD would inhibit pyogranuloma formation *in vivo*. As such, we used $CD11b^{-/-}$ CGD mice in the zymosan peritonitis model. While initial cell recruitment was unimpeded, organized collections of neutrophils at the diaphragm were inhibited, and the absence of CD11b also had a profound effect on MoMac behavior as evidenced by their diminished number at the diaphragm and notable absence within the loose aggregate structures that were present (Figure 6D). The absence of tight neutrophil aggregation at the diaphragm likely decreases the MoMac attractant(s), and indeed, many other inflammatory cytokines and chemokines as well. Although we also predicted a reduction in LTB_4 due to this disruption, levels of the mediator were not different in the bulk PL fluid (data not shown) though may have been reduced in the localized vicinity of the diaphragm. CD11b, in addition to its adhesive functions as an integrin, has also been demonstrated to propagate proinflammatory signaling via the activation of the transcription factor NF-κB.[53] Accordingly, its absence, diminishment, or blockade may result in the reduction of key MoMac attractant(s). Whether CD11b is functioning solely as an adhesion molecule or also as a direct propagator of proinflammatory signaling in our model is an open question and area of further investigation.

Limitations of the study

While this study clearly highlights an important role for LTB_4-BLT1 signaling and CD11b in the formation of pyogranuloma in CGD mice, there are several limitations that should be mentioned. First, while an important role for CD11b was identified, an open question is the specific CD11b ligand that is important in this process. None of the CD11b ligands tested appear to be required for aggregate formation, and we speculate that β-glucan from the zymosan may be released and able to interact with CD11b on the neutrophil surface. Second, while the pyogranuloma both *in vivo* and in our *in vitro* model system contain both neutrophils and MoMacs, and the neutrophils appear to aggregate first and subsequently recruit MoMacs, we were unable to identify the MoMac chemoattractant factor even with a reasonably broad approach. Future studies could use a mass spectrometry-based approach to identify all potential targets in an unbiased manner. Despite these limitations, this study highlights important pathways involved in CGD pyogranuloma formation as well as the identification of important kinetics in this process.

STAR★METHODS

Detailed methods are provided in the online version of this paper and include the following:

- KEY RESOURCES TABLE
- RESOURCE AVAILABILITY
  - Lead contact
  - Materials availability
  - Data and code availability
- EXPERIMENTAL MODEL AND STUDY PARTICIPANT DETAILS
  - *In vivo* mouse model
  - Ex vivo model
- METHOD DETAILS
  - Fluorescence-activated cell sorting
  - Ex vivo aggregation model of pyogranuloma formation
  - Measurement of LTB_4 and chemokine/cytokine levels by ELISA and multiplex assay
  - Transwell assays
  - Tissue collection and immunofluorescence
  - Immunofluorescence of *ex vivo* cultures
  - Live cell time lapse imaging
- QUANTIFICATION AND STATISTICAL ANALYSIS
  - Quantitative microscopy analysis
  - General statistical analysis

SUPPLEMENTAL INFORMATION

Supplemental information can be found online at https://doi.org/10.1016/j.isci.2024.109589.

ACKNOWLEDGMENTS

The authors wish to thank Josh Loomis for technical assistance with the live microscopy experiments and Dr. Scott Thompson for technical assistance and discussions. This work was supported by the National Institute of Allergy and Infectious Diseases (RAI141389, D.L.B., T32 AI740529, K.C.H.) and the National Heart, Lung, and Blood Institute (RHL149741, P.M.H.). All schematics in the figures were generated using BioRender.

AUTHOR CONTRIBUTIONS

Contribution: K.C.H. and S.L.G. collected data; K.C.H., S.L.G., P.M.H., and D.L.B. interpreted the data; J.J. contributed vital new analytical techniques; K.C.H. and D.L.B. wrote the article. All authors helped design the research and edited the article.

DECLARATION OF INTERESTS

The authors declare no competing financial interests.

Received: December 7, 2023
Revised: February 23, 2024
Accepted: March 25, 2024
Published: March 27, 2024

REFERENCES

1. Sacco, K.A., Gazzin, A., Notarangelo, L.D., and Delmonte, O.M. (2023). Granulomatous inflammation in inborn errors of immunity. Front. Pediatr. *11*, 1110115. https://doi.org/10.3389/fped.2023.1110115.
2. Schäppi, M.G., Jaquet, V., Belli, D.C., and Krause, K.H. (2008). Hyperinflammation in chronic granulomatous disease and anti-inflammatory role of the phagocyte NADPH oxidase. Semin. Immunopathol. *30*, 255–271. https://doi.org/10.1007/s00281-008-0119-2.
3. Marciano, B.E., Spalding, C., Fitzgerald, A., Mann, D., Brown, T., Osgood, S., Yockey, L., Darnell, D.N., Barnhart, L., Daub, J., et al. (2015). Common severe infections in chronic granulomatous disease. Clin. Infect. Dis. *60*, 1176–1183. https://doi.org/10.1093/cid/ciu1154.
4. Kuijpers, T., and Lutter, R. (2012). Inflammation and repeated infections in CGD: two sides of a coin. Cell. Mol. Life Sci. *69*, 7–15. https://doi.org/10.1007/s00018-011-0834-z.
5. Morgenstern, D.E., Gifford, M.A., Li, L.L., Doerschuk, C.M., and Dinauer, M.C. (1997). Absence of Respiratory Burst in X-linked Chronic Granulomatous Disease Mice Leads to Abnormalities in Both Host Defense and Inflammatory Response to Aspergillus fumigatus. J. Exp. Med. *185*, 207–218.
6. Petersen, J.E., Hiran, T.S., Goebel, W.S., Johnson, C., Murphy, R.C., Azmi, F.H., Hood, A.F., Travers, J.B., and Dinauer, M.C. (2002). Enhanced Cutaneous Inflammatory Reactions to Aspergillus fumigatus in a Murine Model of Chronic Granulomatous Disease. J. Invest. Dermatol. *118*, 424–429.
7. Gibbings, S.L., Haist, K.C., Nick, H., Frasch, S.C., Glass, T.H., Vestal, B., Danhorn, T., Mould, K.J., Henson, P.M., and Bratton, D.L. (2022). Heightened turnover and failed maturation of monocyte-derived macrophages in murine chronic granulomatous disease. Blood *139*, 1707–1721. https://doi.org/10.1182/blood.2021011798.
8. Henrickson, S.E., Jongco, A.M., Thomsen, K.F., Garabedian, E.K., and Thomsen, I.P. (2018). Noninfectious Manifestations and Complications of Chronic Granulomatous Disease. J. Pediatric Infect. Dis. Soc. *7*, 18–24. https://doi.org/10.1093/jpids/piy014.
9. Dinauer, M.C. (2019). Inflammatory consequences of inherited disorders affecting neutrophil function. Blood *133*, 2130–2139. https://doi.org/10.1182/blood-2018-11-844563.
10. Rosenzweig, S.D. (2008). Inflammatory Manifestations in Chronic Granulomatous Disease (CGD). J. Clin. Immunol. *28*, 67–72. https://doi.org/10.1007/s10875-007-9160-5.
11. Elkington, P., Lerm, M., Kapoor, N., Mahon, R., Pienaar, E., Huh, D., Kaushal, D., and Schlesinger, L.S. (2019). In vitro granuloma models of tuberculosis: Potential and challenges. J. Infect. Dis. *219*, 1858–1866. https://doi.org/10.1093/infdis/jiz020.
12. Algood, H.M.S., Lin, P.L., and Flynn, J.L. (2005). Tumor necrosis factor and chemokine interactions in the formation and maintenance of granulomas in tuberculosis. Clin. Infect. Dis. *41*, 189–193. https://doi.org/10.1086/429994.
13. Crouser, E.D., White, P., Caceres, E.G., Julian, M.W., Papp, A.C., Locke, L.W., Sadee, W., and Schlesinger, L.S. (2017). A novel in vitro human granuloma model of sarcoidosis and latent tuberculosis infection. Am. J. Respir. Cell Mol. Biol. *57*, 487–498. https://doi.org/10.1165/rcmb.2016-0321OC.
14. Klinge, U., Dievernich, A., and Stegmaier, J. (2022). Quantitative Characterization of Macrophage, Lymphocyte, and Neutrophil Subtypes Within the Foreign Body Granuloma of Human Mesh Explants by 5-Marker Multiplex Fluorescence Microscopy. Front. Med. *9*, 777439. https://doi.org/10.3389/fmed.2022.777439.
15. Antmen, E., Muller, C.B., Calligaro, C., Dupret-Bories, A., Barthes, J., Lavalle, P., and Vrana, N.E. (2022). In vitro two-step granuloma formation model for testing innate immune response to implants and coatings. Biomater. Adv. *138*, 212872. https://doi.org/10.1016/j.bioadv.2022.212872.
16. Song, Z., Huang, G., Chiquetto Paracatu, L., Grimes, D., Gu, J., Luke, C.J., Clemens, R.A., and Dinauer, M.C. (2020). NADPH oxidase controls pulmonary neutrophil infiltration in the response to fungal cell walls by limiting LTB4. Blood *135*, 891–903. https://doi.org/10.1182/BLOOD.2019003525.
17. Reátegui, E., Jalali, F., Khankhel, A.H., Wong, E., Cho, H., Lee, J., Serhan, C.N., Dalli, J., Elliott, H., and Irimia, D. (2017). Microscale arrays for the profiling of start and stop signals coordinating human-neutrophil swarming. Nat. Biomed. Eng. *1*, 0094. https://doi.org/10.1038/s41551-017-0094.
18. Walters, N., Zhang, J., Rima, X.Y., Nguyen, L.T.H., Germain, R.N., Lämmermann, T., and Reátegui, E. (2021). Analyzing Inter-Leukocyte Communication and Migration In Vitro: Neutrophils Play an Essential Role in Monocyte Activation During Swarming. Front. Immunol. *12*, 671546. https://doi.org/10.3389/fimmu.2021.671546.
19. Mackiewicz, Z., Rimkevičius, A., Petersen, J., Andersen, C.B., Dudek, E., Vytrasova, M., and Konttinen, Y.T. (2005). Macrophages overloaded with tissue debris in Wegener's granulomatosis. Ann. Rheum. Dis. *64*, 1229–1232. https://doi.org/10.1136/ard.2004.027029.
20. Pagán, A.J., and Ramakrishnan, L. (2018). The Formation and Function of Granulomas. Annu. Rev. Immunol. *36*, 639–665. https://doi.org/10.1146/annurev-immunol-032712-100022.
21. Lämmermann, T., Afonso, P.V., Angermann, B.R., Wang, J.M., Kastenmüller, W., Parent, C.A., and Germain, R.N. (2013). Neutrophil swarms require LTB4 and integrins at sites of cell death in vivo. Nature *498*, 371–375. https://doi.org/10.1038/nature12175.
22. Iizuka, Y., Yokomizo, T., Terawaki, K., Komine, M., Tamaki, K., and Shimizu, T. (2005). Characterization of a mouse second leukotriene B4 receptor, mBLT2: BLT2-dependent ERK activation and cell migration of primary mouse keratinocytes. J. Biol. Chem. *280*, 24816–24823. https://doi.org/10.1074/jbc.M413257200.
23. Matsunaga, Y., Fukuyama, S., Okuno, T., Sasaki, F., Matsunobu, T., Asai, Y., Matsumoto, K., Saeki, K., Oike, M., Sadamura, Y., et al. (2013). Leukotriene B4 receptor BLT2 negatively regulates allergic airway eosinophilia. FASEB J. *27*, 3306–3314. https://doi.org/10.1096/fj.12-217000.
24. Yokomizo, T., Kato, K., Hagiya, H., Izumi, T., and Shimizu, T. (2001). Hydroxyeicosanoids Bind to and Activate the Low Affinity Leukotriene B 4 Receptor, BLT2. J. Biol. Chem. *276*, 12454–12459. https://doi.org/10.1074/jbc.M011361200.
25. Yokomizo, T. (2015). Two distinct leukotriene B4 receptors, BLT1 and BLT2. J. Biochem. *157*, 65–71. https://doi.org/10.1093/jb/mvu078.
26. Alten, R., Gromnica-Ihle, E., Pohl, C., Emmerich, J., Steffgen, J., Roscher, R., Sigmund, R., Schmolke, B., and Steinmann, G. (2004). Inhibition of leukotriene B4-induced CD11B/CD18 (Mac-1) expression by BIIL 284, a new long acting LTB4 receptor antagonist, in patients with rheumatoid arthritis. Ann. Rheum. Dis. *63*, 170–176. https://doi.org/10.1136/ard.2002.004499.
27. Marder, P., Schultz, R.M., Spaethe, S.M., Sofia, M.J., and Herron, D.K. (1992). Flow cytometric evaluation of the effects of leukotriene B4 receptor antagonists (LY255283 and SC-41930) on calcium mobilization and integrin expression of activated human neutrophils. Prostaglandins Leukot. Essent. Fatty Acids *46*, 265–270. https://doi.org/10.1016/0952-3278(92)90033-F.
28. Yakovlev, S., Zhang, L., Ugarova, T., and Medved, L. (2005). Interaction of fibrin(ogen) with leukocyte receptor α Mβ2 (Mac-1): Further characterization and identification of a novel binding region within the central domain of the fibrinogen γ-module. Biochemistry *44*, 617–626. https://doi.org/10.1021/bi048266w.
29. Van Strijp, J.A., Russell, D.G., Tuomanen, E., Brown, E.J., and Wright, S.D. (1993). Ligand specificity of purified complement receptor type three (CD11b/CD18, alpha m beta 2, Mac-1). Indirect effects of an Arg-Gly-Asp (RGD) sequence. J. Immunol. *151*, 3324–3336.
30. Coxon, A., Rieu, P., Barkalow, F.J., Askari, S., Sharpe, A.H., Von Andrian, U.H., Arnaout, M.A., and Mayadas, T.N. (1996). A novel role for the β2 integrin CD11b/CD18 in neutrophil apoptosis: A homeostatic mechanism in inflammation. Immunity *5*, 653–666. https://doi.org/10.1016/S1074-7613(00)80278-2.
31. Arlabosse, T., Booth, C., and Candotti, F. (2023). Gene Therapy for Inborn Errors of Immunity. J. Allergy Clin. Immunol. Pract. *11*, 1592–1601. https://doi.org/10.1038/s41577-022-00800-6.
32. Yang, A.H., Sullivan, B., Zerbe, C.S., De Ravin, S.S., Blakely, A.M., Quezado, M.M., Marciano, B.E., Marko, J., Ling, A., Kleiner, D.E., et al. (2023). Gastrointestinal and Hepatic Manifestations of Chronic Granulomatous Disease. J. Allergy Clin. Immunol. Pract. *11*, 1401–1416. https://doi.org/10.1016/j.jaip.2022.12.039.
33. Bagaitkar, J., Huang, J., Zeng, M.Y., Pech, N.K., Monlish, D.A., Perez-Zapata, L.J., Miralda, I., Schuettpelz, L.G., and Dinauer, M.C. (2018). NADPH oxidase activation regulates apoptotic neutrophil clearance by murine macrophages. Blood *131*, 2367–2378.
34. Fernandez-Boyanapalli, R.F., Frasch, S.C., McPhillips, K., Vandivier, R.W., Harry, B.L., Riches, D.W.H., Henson, P.M., and Bratton, D.L. (2009). Impaired apoptotic cell clearance in CGD due to altered macrophage programming is reversed by phosphatidylserine-dependent production of IL-4. Blood *113*, 2047–2055. https://doi.org/10.1182/blood-2008-05-160564.
35. Sanmun, D., Witasp, E., Jitkaew, S., Tyurina, Y.Y., Kagan, V.E., Åhlin, A., Palmblad, J., and Fadeel, B. (2009). Involvement of a functional

NADPH oxidase in neutrophils and macrophages during programmed cell clearance: Implications for chronic granulomatous disease. Am. J. Physiol. Cell Physiol. *297*, 621–631. https://doi.org/10.1152/ajpcell.00651.2008.

36. Frasch, S.C., Berry, K.Z., Fernandez-Boyanapalli, R., Jin, H.S., Leslie, C., Henson, P.M., Murphy, R.C., and Bratton, D.L. (2008). NADPH oxidase-dependent generation of lysophosphatidylserine enhances clearance of activated and dying neutrophils via G2A. J. Biol. Chem. *283*, 33736–33749. https://doi.org/10.1074/jbc.M807047200.
37. Rybicka, J.M., Balce, D.R., Khan, M.F., Krohn, R.M., and Yates, R.M. (2010). NADPH oxidase activity controls phagosomal proteolysis in macrophages through modulation of the lumenal redox environment of phagosomes. Proc. Natl. Acad. Sci. USA *107*, 10496–10501. https://doi.org/10.1073/pnas.0914867107.
38. Huang, J., Canadien, V., Lam, G.Y., Steinberg, B.E., Dinauer, M.C., Magalhaes, M.A.O., Glogauer, M., Grinstein, S., and Brumell, J.H. (2009). Activation of antibacterial autophagy by NADPH oxidases. Proc. Natl. Acad. Sci. USA *106*, 6226–6231. https://doi.org/10.1073/pnas.0811045106.
39. Peters, N.C., Egen, J.G., Secundino, N., Debrabant, A., Kimblin, N., Kamhawi, S., Lawyer, P., Fay, M.P., Germain, R.N., and Sacks, D. (2008). In Vivo Imaging Reveals an Essential Role for Neutrophils in Leishmaniasis Transmitted by Sand Flies. Science *321*, 970–974.
40. Bruns, S., Kniemeyer, O., Hasenberg, M., Aimanianda, V., Nietzsche, S., Thywissen, A., Jeron, A., Latgé, J.P., Brakhage, A.A., and Gunzer, M. (2010). Production of extracellular traps against aspergillus fumigatus in vitro and in infected lung tissue is dependent on invading neutrophils and influenced by hydrophobin roda. PLoS Pathog. *6*, e1000873. https://doi.org/10.1371/journal.ppat.1000873.
41. Waite, J.C., Leiner, I., Lauer, P., Rae, C.S., Barbet, G., Zheng, H., Portnoy, D.A., Pamer, E.G., and Dustin, M.L. (2011). Dynamic imaging of the effector immune response to listeria infection In Vivo. PLoS Pathog. *7*, e1001326. https://doi.org/10.1371/journal.ppat.1001326.
42. Ng, L.G., Qin, J.S., Roediger, B., Wang, Y., Jain, R., Cavanagh, L.L., Smith, A.L., Jones, C.A., De Veer, M., Grimbaldeston, M.A., et al. (2011). Visualizing the neutrophil response to sterile tissue injury in mouse dermis reveals a three-phase cascade of events. J. Invest. Dermatol. *131*, 2058–2068. https://doi.org/10.1038/jid.2011.179.
43. Chtanova, T., Schaeffer, M., Han, S.J., van Dooren, G.G., Nollmann, M., Herzmark, P., Chan, S.W., Satija, H., Camfield, K., Aaron, H., et al. (2008). Dynamics of Neutrophil Migration in Lymph Nodes during Infection. Immunity *29*, 487–496. https://doi.org/10.1016/j.immuni.2008.07.012.
44. Kienle, K., and Lämmermann, T. (2016). Neutrophil swarming: an essential process of the neutrophil tissue response. Immunol. Rev. *273*, 76–93. https://doi.org/10.1111/imr.12458.
45. Dal-Secco, D., Wang, J., Zeng, Z., Kolaczkowska, E., Wong, C.H.Y., Petri, B., Ransohoff, R.M., Charo, I.F., Jenne, C.N., and Kubes, P. (2015). A dynamic spectrum of monocytes arising from the in situ reprogramming of CCR2+ monocytes at a site of sterile injury. J. Exp. Med. *212*, 447–456. https://doi.org/10.1084/jem.20141539.
46. Strickland, E., Pan, D., Godfrey, C., Kim, J.S., Hopke, A., Degrange, M., Villavicencio, B., Mansour, M.K., Zerbe, C.S., Irimia, D., et al. (2023). Self-extinguishing relay waves enable homeostatic control of human neutrophil swarming. Preprint at bioRxiv *1*. https://doi.org/10.1101/2023.06.27.546744.
47. Hopke, A., Lin, T., Scherer, A.K., Shay, A.E., Timmer, K.D., Wilson-Mifsud, B., Mansour, M.K., Serhan, C.N., Irimia, D., and Hurley, B.P. (2022). Transcellular biosynthesis of leukotriene B4 orchestrates neutrophil swarming to fungi. iScience *25*, 105226. https://doi.org/10.1016/j.isci.2022.105226.
48. Lee, E.K.S., Gillrie, M.R., Li, L., Arnason, J.W., Kim, J.H., Babes, L., Lou, Y., Sanati-Nezhad, A., Kyei, S.K., Kelly, M.M., et al. (2018). Leukotriene B4-Mediated Neutrophil Recruitment Causes Pulmonary Capillaritis during Lethal Fungal Sepsis. Cell Host Microbe *23*, 121–133.e4. https://doi.org/10.1016/j.chom.2017.11.009.
49. Caffrey-Carr, A.K., Hilmer, K.M., Kowalski, C.H., Shepardson, K.M., Temple, R.M., Cramer, R.A., and Obar, J.J. (2017). Host-derived leukotriene B4 is critical for resistance against invasive pulmonary aspergillosis. Front. Immunol. *8*, 1984. https://doi.org/10.3389/fimmu.2017.01984.
50. Hopke, A., Scherer, A., Kreuzburg, S., Abers, M.S., Zerbe, C.S., Dinauer, M.C., Mansour, M.K., Irimia, D., Hopke, A., Scherer, A., et al. (2020). Neutrophil swarming delays the growth of clusters of pathogenic fungi. Nat. Commun. *11*, 2031. https://doi.org/10.1038/s41467-020-15834-4.
51. Mack, M., Cihak, J., Simonis, C., Luckow, B., Proudfoot, A.E., Plachý, J., Brühl, H., Frink, M., Anders, H.-J., Vielhauer, V., et al. (2001). Expression and Characterization of the Chemokine Receptors CCR2 and CCR5 in Mice. J. Immunol. *166*, 4697–4704. https://doi.org/10.4049/jimmunol.166.7.4697.
52. Xia, Y., Větvička, V., Yan, J., Hanikýrová, M., Mayadas, T., and Ross, G.D. (1999). The β-Glucan-Binding Lectin Site of Mouse CR3 (CD11b/CD18) and Its Function in Generating a Primed State of the Receptor That Mediates Cytotoxic Activation in Response to iC3b-Opsonized Target Cells. J. Immunol. *162*, 2281–2290. https://doi.org/10.4049/jimmunol.162.4.2281.
53. Kettritz, R., Choi, M., Rolle, S., Wellner, M., and Luft, F.C. (2004). Integrins and Cytokines Activate Nuclear Transcription Factor-κB in Human Neutrophils. J. Biol. Chem. *279*, 2657–2665. https://doi.org/10.1074/jbc.M309778200.
54. Adams, R.A., Bauer, J., Flick, M.J., Sikorski, S.L., Nuriel, T., Lassmann, H., Degen, J.L., and Akassoglou, K. (2007). The fibrin-derived γ377-395 peptide inhibits microglia activation and suppresses relapsing paralysis in central nervous system autoimmune disease. J. Exp. Med. *204*, 571–582. https://doi.org/10.1084/jem.20061931.
55. Hasenberg, A., Hasenberg, M., Männ, L., Neumann, F., Borkenstein, L., Stecher, M., Kraus, A., Engel, D.R., Klingberg, A., Seddigh, P., et al. (2015). Catchup: A mouse model for imaging-based tracking and modulation of neutrophil granulocytes. Nat. Methods *12*, 445–452. https://doi.org/10.1038/nmeth.3322.

STAR★METHODS

KEY RESOURCES TABLE

REAGENT or RESOURCE	SOURCE	IDENTIFIER
Antibodies		
Anti-Ly6G PE	Biolegend	Cat #127608, Clone 1A8; RRID: AB_1186104
Anti-CD64 PE	Biolegend	Cat #139304, Clone X54-5/7.1; RRID: AB_10612740
Anti-CD19 PE	Biolegend	Cat #152408, Clone 1D3/CD19; RRID: AB_2629816
Anti-CD3e PE	Biolegend	Cat #100308, Clone 145-2C11; RRID: AB_312673
Anti-NK1.1 PE	Biolegend	Cat #108708, Clone PK136; RRID: AB_313394
Anti-SiglecF PE	BD	Cat #552126, Clone E50-2440; RRID: AB_394341
Anti-Tim4 BUV395	BD	Cat #742779, Clone 21H12; RRID: AB_2741043
Anti-CD64 BV711	Biolegend	Cat #139311, Clone X54-5/7.1; RRID: AB_2563846
Anti-CD115 BV605	Biolegend	Cat #135517, Clone AFS98; RRID: AB_2562760
Anti-Ly6G PE-Cy7	Biolegend	Cat #127618, Clone 1A8; RRID: AB_1877262
Anti-Ly6C BV510	Biolegend	Cat #128033, Clone HK1.4; RRID: AB_2562351
Anti-MHCII APC-Cy7	Biolegend	Cat #107628, Clone M5/114.15.2; RRID: AB_2069377
Annexin V APC	Biolegend	Cat #640920
Anti-CD45 BUV395	BD	Cat #564279, Clone 30-F11; RRID: AB_2651134
Anti-Ly6G APC	Biolegend	Cat #127614, Clone 1A8; RRID: AB_2227348
Anti-CD64 PE-Cy7	Biolegend	Cat #139314, Clone X54-5/7.1; RRID: AB_2563903
Anti-CD115 BV711	Biolegend	Cat #135515, Clone AFS98; RRID: AB_2562679
Anti-Ly6G BV421	Biolegend	Cat #127628, Clone 1A8; RRID: AB_2562567
Anti-CD11b AF488	Biolegend	Cat # 101217, Clone M1/70; RRID: AB_389305
Rat IgG2b, κ Isotype AF488	Biolegend	Cat #400625, Clone RTK4530; RRID: AB_389321
Anti-Ly6G BUV395	BD	Cat #563978, Clone 1A8; RRID: AB_2716852
Anti-CD64 AF647	Biolegend	Cat #139322, Clone X54-5/7.1; RRID: AB_2566560
Anti-Ly6G PerCP-Cy5.5	Biolegend	Cat #127616, Clone 1A8; RRID: AB_1877271
Anti-mouse IgG1 AF555	Invitrogen	Cat #A-21127; RRID: AB_2535769
Anti-Rabbit IgG AF555	Invitrogen	Cat #A-21429; RRID: AB_2535850
Anti-CD54 PE-Cy7	Biolegend	Cat #116121, Clone YN1/1.7.4; RRID: AB_2715950
Anti-CD61 AF488	Biolegend	Cat #104311, Clone 2C9.G2; RRID: AB_2128907
Anti-CD11b	BioRad	Clone 5C6
Anti-F4/80	Biolegend	Cat #123102, Clone BM8; RRID: AB_893504
Anti-RFP	Rockland	Cat #200-101-379; RRID: AB_2744552
Anti-Fibrin(ogen)	Agilent	Cat #A008002-2
Anti-Rat IgG AF488	Invitrogen	Cat #A21208; RRID: AB_2535794
Anti-Rabbit IgG AF647	Invitrogen	Cat #A-31573; RRID: AB_2536183
Anti-CCL2	BioXcell	Clone 2H5
Anti-CCL3	R&D Systems	Cat #AB-450-NA; RRID: AB_354363
Anti-CCL4	R&D Systems	Cat #AB-451-NA; RRID: AB_354364
Anti-CXCR2	Novus	Clone 242216
Anti-CD61	Biolegend	Cat #104325, Clone 2C9.G2; RRID: AB_2832322
Anti-C3b	Millipore	Cat #MABF972, Clone 3E7
Anti-ICAM1	BioXcell	Cat #BE0020-1, Clone YN1/1.7.4; RRID: AB_1107661

(*Continued on next page*)

Continued

REAGENT or RESOURCE	SOURCE	IDENTIFIER
Chemicals, peptides, and recombinant proteins		
U75302	Cayman Chemical	Cat #70705
LY255283	Cayman Chemical	Cat #70715
Reparixin L-lysine	R&D Systems	Cat #6957
Boc-MLF	Tocris	Cat #3730
Cyclosporin H	Cayman Chemical	Cat #17182
WRW4	Tocris	Cat #2262
Zymosan A	Sigma	Cat #Z4250
Zymosan A AF488-conjugated	Invitrogen	Cat #Z23373
MK-0812	Cayman Chemical	Cat #21803
BX471	Cayman Chemical	Cat #18503
ML339	Tocris	Cat #5943/10
Scramble peptide (KMMISYTFPIERTGLISNK)	GenScript, sequence from Adams et al.[54]	Custom peptide synthesis
Fibrinogen-γ377-395 (YSMKETTMKIIPFNRLSIG)	GenScript, sequence from Adams et al.[54]	Custom peptide synthesis
SYTOX Blue	ThermoFisher	Cat #S34857
SYTOX Orange	ThermoFisher	Cat #S34861
Critical commercial assays		
LTB_4 ELISA	Cayman Chemical	Cat #520111
LTB_4 ELISA	Enzo Life Sciences	Cat #ADI-900-068
Mouse Proinflammatory Chemokine LEGENDplex	Biolegend	Cat #740451
Mouse Macrophage/Microglia LEGENDplex	Biolegend	Cat #740846
Anti-PE NanoBeads	Biolegend	Cat #480080
Mouse CXCL2/MIP-2 DuoSet ELISA	R&D Systems	Cat #DY452
Experimental models: Organisms/strains		
Mouse: C57BL/6J	The Jackson Laboratory	Jax: 000664
Mouse: CD45.1 (B6.SJL-*Ptprc*^{a}*Pepc*^{b}/BoyJ)	The Jackson Laboratory	Jax: 002014
Mouse: CGD (B6.129S-*Cybb*^{tm1Din}/J)	The Jackson Laboratory	Jax: 002365
Mouse: CD11b$^{-/-}$ (B6.129S4-*Itgam*^{tm1Myd}/J)	The Jackson Laboratory	Jax: 003991
Mouse: BLT1$^{-/-}$ (B6.129S4-*Ltb4r1*^{tm1Adl}/J)	Bryan Yipp	Jax: 008102
Mouse: Catchup (Ly6g$^{Cre\text{-}tdTomato}$)	Matthias Gunzer[55]	N/A
Software and algorithms		
Imaris v8.6.4	Bitplane	https://imaris.oxinst.com/
FlowJo v10.6.2	BD	http://www.flowjo.com
Prism v8.4.3	GraphPad	http://www.graphpad.com

RESOURCE AVAILABILITY

Lead contact

Further information and requests for resources and reagents should be directed to and will be fulfilled by the lead contact, Kelsey Haist (haistk@njhealth.org).

Materials availability

This study did not generate new unique reagents.

Data and code availability

All data reported in this paper will be shared by the lead contact upon request.

This paper does not report original code.

Any additional information required to reanalyze the data reported in this paper is available from the lead contact upon request.

EXPERIMENTAL MODEL AND STUDY PARTICIPANT DETAILS

In vivo mouse model

C57BL/6, CD45.1, gp91$^{phox-/-}$, and CD11b$^{-/-}$ mice were obtained from The Jackson Laboratory and bred in-house in a specific pathogen-free facility at National Jewish Health. BLT1$^{-/-}$ mice were obtained from Bryan Yipp (University of Calgary). Catchup (Ly6G^{Cre}-tdTomato) mice were obtained from Matthias Gunzer (University Duisburg–Essen)[55] and crossed with gp91$^{phox-/-}$ mice to generate Catchup CGD mice. CD11b$^{-/-}$ CGD mice were generated by crossing CD11b$^{-/-}$ mice with gp91$^{phox-/-}$ mice. Male mice 8–12 weeks of age were used for all *in vivo* experiments, modeling X-linked CGD affecting male individuals, and were used in accordance with protocols approved by the Institutional Animal Care and Use Committee (Protocol #: AS2574).

Ex vivo model

Experimental mice were treated with 200 μg zymosan (MilliporeSigma) via intraperitoneal (i.p.) injection. Exudate from both male and female mice 8–12 weeks of age were used for all *ex vivo* experiments.

METHOD DETAILS

Fluorescence-activated cell sorting

Diaphragms were removed, minced with scissors and digested by incubation in 200 μg/mL Liberase TM (Roche/Sigma) for 45 min. Single cell suspensions were made by repeated pipetting and passage through a 100 μm strainer. Single cell suspensions were incubated with anti-CD16/32 antibody before antibody staining (Table S1). Data were acquired on an LSR Fortessa flow cytometer and analyzed using FlowJo software (BD). Dead cells were excluded by using 1 mM SYTOX dyes (Thermo Fisher Scientific).

Ex vivo aggregation model of pyogranuloma formation

Mice were euthanized by CO_2 asphyxiation. Peritoneal lavage was performed by using 8 mL lavage buffer (Hanks balanced salt solution, 10 mM N-2-hydroxyethylpiperazine-N′-2-ethanesulfonic acid, 1 mM ethylenediaminetetraacetic acid). Cells were passed through a 70 μm strainer to ensure a single cell suspension. Cells were counted, resuspended in culture medium (Roswell Park Memorial Institute 1640 Medium supplemented with 10% fetal bovine serum, 100 U/mL of penicillin, 100 U/mL of streptomycin, and 29.2 mg/mL of L-glutamine), and plated at a density of 1×10^6 cells/well in 24-well plates. Where indicated, cells were plated in the presence of the following antagonists or antibodies at the time of plating: 8 μg/mL U-75302, 83.3 μM LY255283, 5 μM reparixin L-lysine, 1 μM Boc-MLF, 1 μM cyclosporin H, 1 μM WRW4, 10 μg/mL anti-CD11b (clone 5C6), 10 μg/mL anti-CCL2 (clone 2H5), 10 μg/mL anti CCL3 (polyclonal, R&D Systems), and 10 μg/mL anti-CCL4 (polyclonal, R&D Systems). Isotype control antibodies were used as controls for each of the neutralizing antibodies at the corresponding concentrations. Vehicle controls (ethanol for U-75302, DMSO for LY255283, reparixin L-lysine, Boc-MLF, and cyclosporin H, and water for WRW4) were used as controls for the antagonist treatments at the corresponding concentrations of vehicle. Cells were cultured at 37°C with 5% CO_2 for up to 24 h.

Measurement of LTB_4 and chemokine/cytokine levels by ELISA and multiplex assay

LTB_4 levels in peritoneal lavage fluid and cell culture supernatants were analyzed by commercially available ELISAs (Cayman or Enzo Life Sciences). CXCL2 levels in cell culture supernatants were analyzed by commercially available ELISA kit (R&D Systems). All other cytokines and chemokines were measured using a LEGENDplex assay (BioLegend).

Transwell assays

Six hours post-zymosan, CGD peritoneal lavage (PL) cells were plated (1×10^6 cells/well in 24-well plates) and cultured for 24 h to condition media for the transwell assay. Peritoneal exudate was collected 20 h post-zymosan, and MoMacs were enriched via negative selection using a MojoSort Anti-PE Beads kit (BioLegend) and PE-conjugated antibodies to CD19, Ter119, Siglec-F, CD3e, NK1.1, and Ly6G. The MoMacs were plated in 24-well plates above the insert. MoMacs were plated in the presence of the following antagonists or neutralizing antibodies as noted: 10 μg/mL anti-CCL2 (clone 2H5), 10 μg/mL anti-CCL3 (polyclonal, R&D Systems), 10 μg/mL anti-CCL4 (polyclonal, R&D Systems), 5 μg/mL anti-CXCR2 (clone 242216), 10 mg/mL MK-0812 (CCR2 and CCR5), 25 mg/mL BX471 (CCR1), and 100 mM ML339 (CXCR6). Isotype control antibodies were used as controls for each of the neutralizing antibodies at the corresponding concentrations. Vehicle controls (ethanol for MK-0812, DMSO for all others) were used as controls for the antagonist treatments at the corresponding concentrations of vehicle. MoMacs migrating beneath a 5 μm transwell insert (Corning) were counted as noted after plating.

Tissue collection and immunofluorescence

Mice were euthanized and PL performed. Diaphragms were removed to be cryopreserved and fixed in 2% paraformaldehyde, 20% sucrose before freezing in Optimal Cutting Temperature media (Tissue-Tek; Sakura Finetek). Cryosections were stained with primary antibodies followed by secondary antibodies (Table S1). 49,6-Diamidino-2-phenylindole (DAPI) was used to stain nuclei. Sections were imaged at 20× or 40× magnification using an Olympus VS200 microscope.

Immunofluorescence of *ex vivo* cultures

Cells grown on coverslips were fixed with 4% paraformaldehyde and then stained. Coverslips were imaged either at 10× magnification using an Olympus VS200 microscope or at 40× magnification using a Zeiss LSM confocal microscope.

Live cell time lapse imaging

Cells were plated on a chamber slide at a density of 1.5×10^6 cells/chamber in Leibovitz's L-15 medium supplemented with 10% fetal bovine serum, 100 U/mL of penicillin, and 100 U/mL of streptomycin and were time lapse imaged every 5 minutes at 20× magnification for 6 hours at 37°C using a Marianas spinning disk microscope.

QUANTIFICATION AND STATISTICAL ANALYSIS

Quantitative microscopy analysis

Images were analyzed blinded using Imaris 8.6.4 software (Bitplane) to quantify number of aggregates, size of aggregates, and percent of MoMacs recruited to aggregates. Aggregates were defined within the software as surfaces that were larger than 381 pixels, which equates to approximately 15 cells. In some experiments, exogenous MoMacs were labeled with carboxyfluorescein succinimidyl ester (CFSE) prior to being added to cultures and defined in the software as spots approximately 1 cell in size. MoMacs were determined to have been recruited to an aggregate if the CFSE-positive spot fell within 1 pixel of an aggregate (surface).

General statistical analysis

All data were analyzed using GraphPad Prism 8 software. Data were evaluated for statistically significant differences using a paired t-test, an unpaired t-test, or a one-way analysis of variance (ANOVA) test followed by Tukey's or Dunnett's multiple comparisons test as indicated in the figure legend. A p value <0.05 was considered statistically significant. The p values are indicated as follows: *$p < 0.05$, **$p < 0.01$, ***$p < 0.001$, ****$p < 0.0001$. A detailed breakdown of values from statistical analyses for each figure is provided in a supplemental file.